A multiscale approach for the vibration analysis of heterogeneous materials: Application to passive damping

Kodjo Attipou, Saeid Nezamabadi, El Mostafa Daya, Hamid Zahrouni

A multiscale approach for the vibration analysis of heterogeneous materials: Application to passive damping

Kodjo Attipou [a], Saeid Nezamabadi [b,*], El Mostafa Daya [a], Hamid Zahrouni [a]

[a] *Université de Lorraine, Laboratoire d'Étude des Microstructures et de Mécanique des Matériaux (LEM3), UMR CNRS 7239, Ile du Saulcy F-57045, Metz Cedex 01, France*
[b] *Université Montpellier 2, Laboratoire de Mécanique et Génie Civil (LMGC), UMR CNRS 5508, CC048 Place Eugène Bataillon, 34095 Montpellier Cedex 05, France*

This paper presents a multiscale numerical technique for vibration analysis of hetero-geneous materials. In this procedure, the unknown macroscopic constitutive relationship is searched by solving a local finite element problem at the microscale. Since the inertia effects are neglected at the microscopic level, this approach is limited to problems in which microstructure characteristic length is smaller than the wavelength. Numerical examples are limited to free vibration analysis of viscoelastic materials with a constant complex modulus. These examples allow one to validate the multiscale approach and to study the influence of different parameters on the passive damping of the structure. These parameters concern the morphology, the stiffness ratio and the inclusion volume fraction.

1. Introduction

Vibrations of structures may cause many problems such as structural fatigue, vibration transmission to other systems and internal or external noises due to acoustic radiation. It is important to reduce these problems in order to increase the lifetime of industrial structures. Vibration analysis is then an important issue which interests many fields in industry such as aerospace and civil construction. This analysis leads to develop the techniques to control structural vibrations. One of these techniques, called passive damping, is to add viscoelastic materials in structures in order to absorb vibration energy thanks to its damping properties. It is an efficient technique to increase structural damping to control vibration modes in a large band of frequencies. Indeed, viscoelastic layer is usually implemented as a constrained layer damping to provide an efficient damping. This is due to its shear deformation, thus dissipating energy in a more efficient way. The other technique to control structural vibrations is the active control of vibrations via electro/magneto-mechanical coupling. One can also combine active and passive damping treatments which is called hybrid control. However, both controls which are efficient at few vibration modes depend strongly on the electric energy provided by the coupling. This limits the control at few modes. A detailed review on active, passive and hybrid solutions can be found in Trindade and Benjeddou [1].

Many interesting studies have been developed for linear vibration analysis of sandwich structures with viscoelastic and/or piezoelectric layers. The first study has been carried out by Kerwin [2]. The main objective was to develop analytical or numerical methods for determining the damping properties of these structures. Indeed, the viscoelastic and/or piezoelectric constitutive laws lead to nonlinear and/or complex eigenvalue problems when dealing with free vibration of

* Corresponding author.
E-mail address: saeid.nezamabadi@univ-montp2.fr (S. Nezamabadi).

sandwich structures. Hence, since the determination of damping properties (modal frequencies and loss factors) is not direct and it cannot be usually performed by commercial codes like ABAQUS®, several methods have been proposed, such as the direct frequency response method [3], the complex eigenvalue method [4,5], the modal strain energy method [6], the asymptotic method [7], the iterative order-reduction method [8] and the asymptotic numerical method (ANM) [9–11]. From these studies, one can note that the passive damping efficiency depends strongly on the viscoelastic core material and the geometrical data of the sandwich structures. In order to improve this damping, the viscoelastic microstructures can be considered in the core like in Refs. [12,13].

To give the macroscopic overall response of heterogeneous materials with complex microstructures in an averaged or homogenized sense, various homogenization techniques are typically used. In the case of material multiscale modelling and in homogenization in general, one usually proceeds from the lower scales upward, in order to obtain equivalent material properties (e.g. [14–20]). Several homogenization techniques of viscoelastic materials have been developed. Christensen [21] proposed an approximate formula for the effective complex shear modulus in the case of materials with two viscoelastic phases by using the composite sphere model. Koishi et al. [22] developed a homogenization method for composite materials in order to predict effective dynamic viscoelastic material properties in the frequency domain. Yi et al. [23] applied the asymptotic homogenization into viscoelastic composites in order to determine the effective moduli. An inverse homogenization problem based on the asymptotic homogenization for two-phase viscoelastic composites was formulated as a topology optimization problem by Yi et al. [24]. Chung et al. [25] developed a micro/macro asymptotic homogenization approach for the analysis of viscoelastic creep in heterogeneous materials. The size effect of the basic cell upon the vibration performances of sandwich beams was studied by Dai and Zhang [26]. Finally, an extended finite element method proposed (X-FEM) by Zhang and Li [27] allows modelling inclusions in viscoelastic materials.

In this paper, we propose a multiscale analysis of damping properties for sandwich structures with viscoelastic inclusions. The main objective is to develop a numerical method for designing sandwich structures with optimized damping properties. Moreover, since the proposed procedure is a numerical homogenization method contrary to the analytical techniques, e.g. asymptotic homogenization, which are usually restricted to very simple microscopic geometries and simple material models (see for example [15,19]), more complex microstructures can then be considered. Furthermore, for simplicity, we consider in this study a simple viscoelastic behaviour with a constant complex modulus like in references [3,7,9,11,28,29] and we suppose that the microscopic inertia effects can be neglected (see e.g. [12]). The first assumption is certainly a simplest way to take account of the viscoelastic behaviour and the second one limits our technique to the low or medium frequency range; but, the methodology can be extended to the more general viscoelastic model by considering the microscopic inertia effects, using numerical techniques for extracting the damping properties such as the ANM algorithms [9–11]. In this context, we present the multiscale formulation of the vibration problem in Section 2. In Section 3, the strategy to solve the vibration multiscale problem is demonstrated. Section 4 is devoted to numerical examples.

2. Multiscale formulation of the vibration problem

2.1. Problem at the macroscopic scale

We consider a domain Ω in $\mathbb{R}^D$, D being the domain dimension, with an external boundary $\partial\Omega$, describing the structure at the macroscopic level. We assume that the material is heterogeneous and characterized by a periodic microstructure. The structure is subjected to prescribed displacements and forces on the disjoint complementary parts of the boundary $\partial\Omega_u$ (the Dirichlet boundaries) and $\partial\Omega_f$ (the Neumann boundaries), respectively. In the following, the notation $\overline{(\cdot)}$ will be used to denote macroscopic quantities. In the context of the infinitesimal strain theory, the problem to solve is defined as follows, in the absence of body forces

$$\boldsymbol{\nabla}\cdot\overline{\boldsymbol{\sigma}} = \overline{\rho}\frac{\partial^2\overline{\mathbf{u}}}{\partial t^2} \quad \text{in } \Omega, \tag{1}$$

where $\overline{\boldsymbol{\sigma}}$ is the macroscopic Cauchy stress tensor and $\overline{\rho}$ indicates the material density. $\overline{\mathbf{u}}$ denotes the macroscopic displacement field. The boundary conditions are defined by

$$\begin{cases} \overline{\mathbf{u}}(\overline{\mathbf{X}}) = \hat{\mathbf{u}}(\overline{\mathbf{X}}) & \text{on } \partial\Omega_u, \\ \overline{\boldsymbol{\sigma}}\cdot\mathbf{N} = \mathbf{f} & \text{on } \partial\Omega_f, \end{cases} \tag{2}$$

where $\hat{\mathbf{u}}$ are the prescribed displacements and $\overline{\mathbf{X}}$ being the coordinates of a given point in the structure. In Eq. (2), $\mathbf{N}$ is the outward unit normal vector to $\partial\Omega$ and $\mathbf{f}$ is a prescribed load. The weak form associated with Eqs. (1) and (2) is given by:

Find $\overline{\mathbf{u}} \in \mathcal{S}(\Omega)$, $\overline{\mathbf{u}} = \hat{\mathbf{u}}$, on $\partial\Omega_u$ such that

$$\int_\Omega \overline{\boldsymbol{\sigma}} : \boldsymbol{\delta}\overline{\boldsymbol{\epsilon}}\, \mathrm{d}\Omega + \int_\Omega \overline{\rho}\frac{\partial^2\overline{\mathbf{u}}}{\partial t^2}\cdot\boldsymbol{\delta}\overline{\mathbf{u}}\, \mathrm{d}\Omega = \int_{\partial\Omega_f} \mathbf{f}\cdot\boldsymbol{\delta}\overline{\mathbf{u}}\, \mathrm{d}\Gamma \ \forall \boldsymbol{\delta}\overline{\mathbf{u}} \in \mathcal{S}_0(\Omega), \tag{3}$$

where $\mathcal{S}(\Omega)$ denotes the space of sufficiently regular displacements and $\mathcal{S}_0(\Omega) = \{\boldsymbol{\delta}\overline{\mathbf{u}} \in \mathcal{S}(\Omega), \boldsymbol{\delta}\overline{\mathbf{u}} = 0 \text{ on } \partial\Omega_u\}$ is the corresponding space of suitable variations with vanishing values on the Dirichlet boundary. Let $\overline{\boldsymbol{\epsilon}} = \frac{1}{2}(\boldsymbol{\nabla}\overline{\mathbf{u}} + {}^t\boldsymbol{\nabla}\overline{\mathbf{u}})$

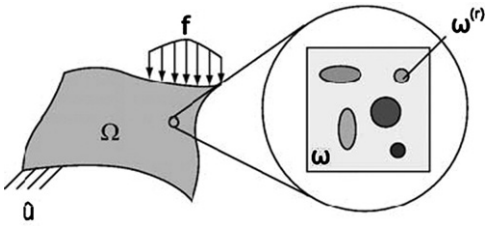

Fig. 1. Multiscale problem schema.

the macroscopic strain tensor. At this scale, the constitutive relationship between $\overline{\boldsymbol{\sigma}}$ and $\overline{\boldsymbol{\epsilon}}$ is unknown. In the context of multiscale analysis, the macroscopic stresses are extracted directly by solving a local finite element problem corresponding to the periodic microstructure (Fig. 1).

2.2. Problem at the microscopic scale

We assume that the material is heterogeneous with a periodic microstructure, characterized by a representative volume element (RVE) that occupies a domain ω in $\mathbb{R}^D$ with external boundary $\partial\omega$. The equilibrium equation is given in the absence of body forces and the inertia effects by the following relation:

$$\boldsymbol{\nabla}\cdot\boldsymbol{\sigma}=0 \quad \text{in } \omega, \tag{4}$$

where $\boldsymbol{\sigma}$ is the microscopic Cauchy stress tensor. Note that the inertia effects are neglected at the microscopic level like in [12,22,24]. This assumption allows us to obtain the macroscopic constitutive relation, i.e. a numerical micro-to-macro transition. However, it limits the present approach to vibration problem in which the microstructure size is smaller than the wavelength. The weak form associated with the microscopic problem is then written as

Find $\mathbf{u}\in\mathcal{S}(\omega)$, with respect to microscopic boundary condition, such that

$$\int_{\omega}\boldsymbol{\sigma}:\boldsymbol{\delta\epsilon}\,\mathrm{d}\omega=0 \quad \forall\boldsymbol{\delta}\mathbf{u}\in\mathcal{S}_0(\omega), \tag{5}$$

where $\boldsymbol{\epsilon}$ denotes the strain tensor at the microscopic scale and $\mathbf{u}$ is the microscopic displacement field.

2.3. Coupling relations and microscopic boundary conditions

Problems (3) and (5) are coupled through two main relations. First, as the constitutive relation is not explicitly given at the macroscopic level, the effective stress tensor $\overline{\boldsymbol{\sigma}}$ is obtained by considering an average value of the microscopic stress field over the RVE for a given point $\overline{\mathbf{X}}$ of the macroscopic structure. This relation is expressed as follows:

$$\overline{\boldsymbol{\sigma}}=\langle\boldsymbol{\sigma}\rangle=\frac{1}{|\omega|}\int_{\omega}\boldsymbol{\sigma}\,\mathrm{d}\omega, \tag{6}$$

where $|\omega|$ represents the volume of the considered RVE.

The second relation concerns the mean value of the microscopic strain assumed in the following form:

$$\overline{\boldsymbol{\epsilon}}=\langle\boldsymbol{\epsilon}\rangle=\frac{1}{|\omega|}\int_{\omega}\boldsymbol{\epsilon}\,\mathrm{d}\omega. \tag{7}$$

This relation follows from the boundary conditions imposed on the RVE which depends on the macroscopic strain tensor $\overline{\boldsymbol{\epsilon}}$. Different types of microscopic boundary conditions can be chosen such as linear deformations, uniform tractions, or periodic constraints (see e.g. [30]). We consider, in this work, the periodic conditions on the boundary of the RVE:

$$\mathbf{u}^{+}-\mathbf{u}^{-}=\overline{\boldsymbol{\epsilon}}\cdot(\mathbf{X}^{+}-\mathbf{X}^{-}) \quad \text{on } \partial\omega \tag{8}$$

The exponents $+$ and $-$ are associated with nodes indices on opposite sides of the RVE (see Fig. 2). Note that the boundary conditions depend on the macroscopic deformation tensor $\overline{\boldsymbol{\epsilon}}$.

2.4. Microscopic constitutive relations

At the microscopic scale, the constitutive relations are known for each phase of the RVE. For simplicity, we suppose that each phase of the RVE is linear, homogeneous, isotropic and elastic or viscoelastic. So, the stress–strain law can be written

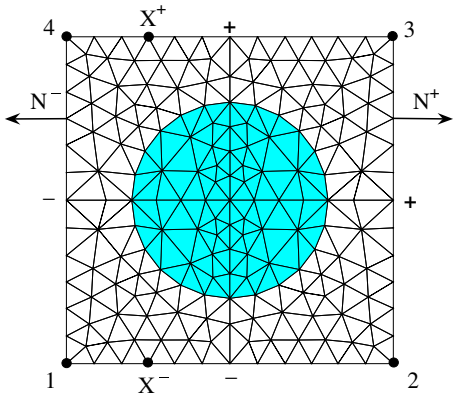

Fig. 2. RVE with periodic boundary conditions.

in the following form:

$$\begin{cases} \sigma = 2\mu\boldsymbol{\epsilon} + \lambda(\boldsymbol{\epsilon} : \mathbf{I})\mathbf{I}, \\ \mu = \dfrac{E}{(1+v)}, \\ \lambda = \dfrac{vE}{(1+v)(1-2v)}, \end{cases} \tag{9}$$

where E is a complex Young's modulus, $\mathbf{I}$ being the second-order identity tensor and v denotes Poisson's ratio which is assumed to be constant, as in most analysis. The complex Young's modulus usually depends on frequency and temperature; but, here, to simplify the presentation, the following complex Young's modulus is chosen:

$$E = E_0(1 + \mathbf{i}\eta_c), \tag{10}$$

where E_0 is the real elastic modulus, η_c denotes the viscoelastic material loss factor and $\mathbf{i}^2 = -1$. Note that, by setting $\eta_c = 0$, the classical Hooke's law will be obtained.

3. Resolution strategy

We present in this section the strategy to solve the presented multiscale problems (Eqs. (3), (5), (6), (8) and (9)). Because of the coupling conditions between macroscopic and microscopic problems, we start by solving partly the linear microscopic problem. The obtained solution allows one to construct the localization tensor numerically and then, to obtain the macroscopic tangent modulus.

In the context of vibration, there are usually two problem types: free and forced vibration problems. For the free vibration problem, by using the obtained macroscopic tangent modulus, a macroscopic eigenvalue problem to solve is obtained. This eigenvalue problem gives the macroscopic natural frequencies and their modes. In the case of forced vibration, one can solve the macroscopic equilibrium problem to obtain the displacement field $\overline{\mathbf{u}}$. This displacement is then used to compute the macroscopic strain $\overline{\boldsymbol{\epsilon}}$ and to finish the computation of the variables at the microscopic level.

3.1. Localization tensors

We solve first numerically the linear microscopic problem by considering the coupling conditions. The solution of the microscopic problem depends linearly on the imposed macroscopic strain. Hence, we can obtain the localization tensor, which allows expressing the microscopic strain with respect to the macroscopic one. The microscopic problem can be defined as follows:

$$\begin{cases} \int_\omega^t \boldsymbol{\sigma} : \boldsymbol{\delta\epsilon}\ \mathrm{d}\omega = 0, \\ \boldsymbol{\sigma} = \mathbf{C}^{(r)} : \boldsymbol{\epsilon}, \qquad + \text{B.C.} : \ \mathbf{u}^+ - \mathbf{u}^- = \overline{\boldsymbol{\epsilon}} \cdot (\mathbf{X}^+ - \mathbf{X}^-) \quad \text{on } \partial\omega \\ \boldsymbol{\epsilon} = \frac{1}{2}(\boldsymbol{\nabla}\mathbf{u} + {}^t\boldsymbol{\nabla}\mathbf{u}), \end{cases} \tag{11}$$

where $\mathbf{C}^{(r)}$ is the fourth-order material constitutive tensor associated with phase (r). In this formulation, only the displacement vector will be discretized in the context of the finite element method. Hence, the substitution of the constitutive relation into the equilibrium one gives

$$\begin{aligned} &\mathcal{L}(\mathbf{u}, \boldsymbol{\delta u}) = 0 \quad \text{in } \omega + \text{B.C.} : \\ &\mathbf{u}^+ - \mathbf{u}^- = \overline{\boldsymbol{\epsilon}} \cdot (\mathbf{X}^+ - \mathbf{X}^-) \quad \text{on } \partial\omega, \end{aligned} \tag{12}$$

where

$$\mathcal{L}(\mathbf{u},\boldsymbol{\delta u}) = \int_{\omega}^{t} \boldsymbol{\delta\epsilon} : \mathbf{C}^{(r)} : \boldsymbol{\epsilon}\, \mathrm{d}\omega. \tag{13}$$

As the problem is linear, its solution, $\mathbf{u}$, can be decomposed into modes associated with different microscopic boundary condition responses. Hence, in the 2D case, we can write through the methodology which can be readily extended to a three-dimensional case

$$\mathbf{u} = \overline{\epsilon}_{11}\tilde{\mathbf{u}}^{(11)} + \overline{\epsilon}_{22}\tilde{\mathbf{u}}^{(22)} + 2\overline{\epsilon}_{12}\tilde{\mathbf{u}}^{(12)} \quad \text{in } \omega, \tag{14}$$

where $\tilde{\mathbf{u}}^{(ij)}$ are the solutions of the following problems:

$$\begin{cases} \mathcal{L}(\tilde{\mathbf{u}}^{(ij)},\boldsymbol{\delta u}) = 0 & \text{in } \omega, \\ \tilde{\mathbf{u}}^{(ij)} - \tilde{\mathbf{u}}^{(ij)} = \mathbf{X}^{(ij)} & \text{on } \partial\omega, \end{cases} \tag{15}$$

with

$$\mathbf{X}^{(11)} = \begin{bmatrix} 1 & 0 \\ 0 & 0 \end{bmatrix} (\mathbf{X}^{+} - \mathbf{X}^{-}),$$

$$\mathbf{X}^{(22)} = \begin{bmatrix} 0 & 0 \\ 0 & 1 \end{bmatrix} (\mathbf{X}^{+} - \mathbf{X}^{-}),$$

$$\mathbf{X}^{(12)} = \frac{1}{2}\begin{bmatrix} 0 & 1 \\ 1 & 0 \end{bmatrix} (\mathbf{X}^{+} - \mathbf{X}^{-}).$$

The exponents (ij) simply indicate that the sought response is related to the component $\overline{\epsilon}_{ij}$ of the macroscopic strain tensor. Finally, the solution $\mathbf{u}$ can be written as follows:

$$\mathbf{u} = \mathbf{A} : \overline{\boldsymbol{\epsilon}}, \tag{16}$$

where $\mathbf{A}$ is the third-order tensor defined by $A_{ijk} = \tilde{u}_i^{(jk)}$. The introduction of Eq. (16) in the definition of microscopic strain tensor, $\boldsymbol{\epsilon}$, gives

$$\boldsymbol{\epsilon} = \mathbf{A}_{,X} : \overline{\boldsymbol{\epsilon}}, \tag{17}$$

where $\mathbf{A}_{,X} = \frac{1}{2}(\boldsymbol{\nabla}\mathbf{A} + {}^{t}\boldsymbol{\nabla}\mathbf{A})$ is the fourth-order tensor identified as the localization tensor.

3.2. Homogenization tensor and macroscopic problem to solve

To obtain the macroscopic homogenized stress–strain law, we consider Eq. (11_2):

$$\boldsymbol{\sigma} = \mathbf{C}^{(r)} : \boldsymbol{\epsilon}. \tag{18}$$

Substituting relation (17) into (18) gives

$$\boldsymbol{\sigma} = (\mathbf{C}^{(r)} : \mathbf{A}_{,X}) : \overline{\boldsymbol{\epsilon}}. \tag{19}$$

The effective stresses can be obtained by averaging Eq. (19)

$$\overline{\boldsymbol{\sigma}} = \overline{\mathbf{C}} : \overline{\boldsymbol{\epsilon}} \tag{20}$$

where $\overline{\mathbf{C}}$ is the fourth-order homogenization tensor defined as

$$\overline{\mathbf{C}} = \frac{1}{|\omega|}\int_{\omega} \mathbf{C}^{(r)} : \mathbf{A}_{,X}\, \mathrm{d}\omega.$$

By introducing (20) into (3), we obtain the final form of the macroscopic problem:

$$\int_{\Omega} \boldsymbol{\delta\overline{\epsilon}} : \overline{\mathbf{C}} : \overline{\boldsymbol{\epsilon}}\, \mathrm{d}\Omega + \int_{\Omega} \boldsymbol{\delta\overline{u}} \cdot \overline{\rho}\frac{\partial^2 \overline{\mathbf{u}}}{\partial t^2}\, \mathrm{d}\Omega = \int_{\partial\Omega_f} \mathbf{f} \cdot \boldsymbol{\delta\overline{u}}\, \mathrm{d}\Gamma. \tag{21}$$

The problem (21) can be solved by the finite element method. As mentioned before, here, the free and forced vibration problems are considered. In the context of free vibration ($\mathbf{f} = 0$), after the finite element discretization of this problem, we can obtain the classical complex eigenvalue problem at the macroscopic level

$$(\overline{\mathbf{K}} - \overline{\omega}^2\overline{\mathbf{M}})\overline{\mathbf{u}} = 0, \tag{22}$$

where $\overline{\mathbf{K}}$ is a complex macroscopic stiffness matrix and $\overline{\mathbf{M}}$ denotes the macroscopic mass matrix. $\overline{\omega}$ represents the structure natural frequency. The amplitude Eq. (22) leads to an approximate complex eigenfrequency that can be written in the following classical form:

$$\overline{\omega}^2 = \overline{\Omega}^2(1 + \mathbf{i}\eta), \tag{23}$$

where $\overline{\Omega}$ is the damped frequency and η is the loss factor of each vibration mode. Furthermore, in the case of forced vibration ($\mathbf{f}\neq 0$), the discretized problem may be given as follows:

$$(\overline{\mathbf{K}}-\lambda^2\overline{\mathbf{M}})\overline{\mathbf{u}}=\mathbf{F}(\lambda,t), \tag{24}$$

where λ is the excitation frequency and $\mathbf{F}$ denotes the prescribed force depending on λ and time, t. Solution $\overline{\mathbf{u}}$ of (24) and Eq. (16) are used to finish the computation of the variables at the microscopic level for each integration point of the macroscopic structure.

Box 1–Summary of the homogenization procedure.

(i): Expand $\mathbf{u}$ as a linear form of $\overline{\boldsymbol{\epsilon}}$ (Eq. (16)) :

$$\mathbf{u}=\mathbf{A}:\overline{\boldsymbol{\epsilon}}$$

(ii): Construct the localization tensors $\mathbf{A_X}$ (Eq. (17)):

$$\boldsymbol{\epsilon}=\mathbf{A}_X:\overline{\boldsymbol{\epsilon}}$$

(iii): Express $\boldsymbol{\sigma}$ using the known constitutive relationship at the micro level (Eq. (19)):

$$\boldsymbol{\sigma}=(\mathbf{C}^{(r)}:\mathbf{A}_X):\overline{\boldsymbol{\epsilon}}$$

(iv): Average to find the effective constitutive law (Eq. (20)):

$$\overline{\boldsymbol{\sigma}}=\overline{\mathbf{C}}:\overline{\boldsymbol{\epsilon}}$$

The layout of the homogenization procedure is summarized in Box 1.

4. Numerical examples

We study the accuracy and the efficiency of the proposed multiscale technique through several numerical examples. The results are presented here through two free vibration examples. The first one concerns the vibration of a viscoelastic heterogeneous beam. It is used to show the validity of the proposed multiscale algorithm. This approach is validated by comparing it with a fully meshed model. In this latter, details of all heterogeneities are meshed. In the second example, we applied the multiscale approach to the vibration analysis of a viscoelastic sandwich beam. The proposed problems have been discretized using two-dimensional finite element in the plane stress framework.

4.1. Heterogeneous beam

To assess the validity of our multiscale approach for vibration analysis, free vibration of a cantilever beam is studied. Dimensions and characteristics of the beam are given in Table 1. The beam is assumed to be heterogeneous and the heterogeneities are represented by viscoelastic circular inclusions into an elastic matrix (Fig. 3a).

In this example, the obtained results with our multiscale procedure are compared to those of a fully meshed structure involving the explicit mesh of all heterogeneities (see Fig. 3b). The full mesh of the beam involves a three-node triangular element, while in the second method, we have used a three-node triangular element to mesh the microstructure and a nine-node quadrangular element to mesh the macrostructure. This latter discretized using 80 elements (20×4). The inclusion represents 28 percent of the RVE. By considering the relation of the constitutive tensor in the context of the plane stress framework:

$$\mathbb{C}=\frac{E}{1-\nu^2}\begin{bmatrix}1 & \nu & 0\\ \nu & 1 & 0\\ 0 & 0 & \dfrac{1-\nu}{2}\end{bmatrix},$$

the effective constitutive tensor, $\overline{\mathbb{C}}$, is shown in Table 2. Moreover, natural frequencies and loss factors obtained from two methods are presented in Table 3. Although the proposed multiscale procedure can reproduce with good accuracy the complete detailed heterogeneous structure response, there is a little difference between the results of two methods. This difference may be due to macroscopic boundary condition effects; i.e. near the macroscopic boundary condition, the periodic microstructure

Table 1
Material properties and beam dimensions for Example 1.

Matrix material properties	
Young's modulus	$E_m = 1000$ MPa
Poisson's ratio	$\nu_m = 0.45$
Density	$\rho_m = 1550$ kg/m^3
Inclusion material properties	
Young's modulus	$E_i = 17940$ kPa
Poisson's ratio	$\nu_i = 0.3$
Density	$\rho_i = 968.1$ kg/m^3
Loss factor	$\eta_c = 0.6$
Beam dimensions	
Length	$L = 200$ mm
Thickness	$h = 40$ mm

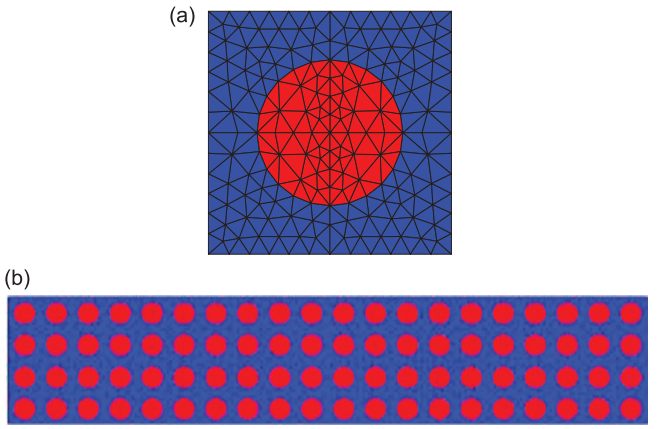

Fig. 3. (a) Biphasic RVE: inclusion volume fraction is 28% and (b) full mesh of the beam using this RVE.

Table 2
Constitutive parameters of cantilever beam for Example 1 ($\eta_c = 0.6$).

$\mathbb{C}_{\text{Matrix}}$ (MPa)	$\begin{bmatrix} 1253.92 & 564.26 & 0 \\ 564.26 & 1253.92 & 0 \\ 0 & 0 & 344.83 \end{bmatrix}$
$\mathbb{C}_{\text{Inclusion}}$ (MPa)	$\begin{bmatrix} 19.71+11.83\mathbf{i} & 5.91+3.55\mathbf{i} & 0 \\ 5.91+3.55\mathbf{i} & 19.71+11.83\mathbf{i} & 0 \\ 0 & 0 & 6.90+4.14\mathbf{i} \end{bmatrix}$
$\overline{\mathbb{C}}$ (MPa)	$\begin{bmatrix} 603.64+11.48\mathbf{i} & 194.67+6.37\mathbf{i} & 0 \\ 194.67+6.37\mathbf{i} & 603.64+11.48\mathbf{i} & 0 \\ 0 & 0 & 140.24+5.44\mathbf{i} \end{bmatrix}$

Table 3
Natural frequencies and loss factors of cantilever beam for Example 1 ($\eta_c = 0.6$).

Fully meshed model		Multiscale method		Dif.% (f)	Dif.% (η/η_c)
f (Hz)	η/η_c	f (Hz)	η/η_c		
97.57	0.0296	97.00	0.0293	0.59	0.93
505.74	0.0389	502.62	0.0385	0.61	1.10
1174.68	0.0451	1166.68	0.0442	0.68	1.92
1914.61	0.0505	1901.02	0.0486	0.71	3.71

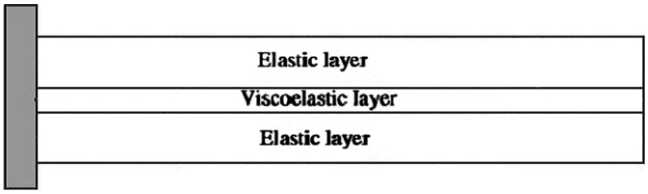

Fig. 4. Cantilever sandwich beam.

Table 4
Material properties and beam dimensions for Example 4.2.

Elastic layers	
Young's modulus	$E_0 = 69$ GPa
Poisson's ratio	$\nu = 0.3$
Density	$\rho_0 = 2766$ kg/m^3
Thickness	$h_0 = 1.524$ mm
Viscoelastic layer	
Matrix elastic modulus	$E_1 = 1794$ KPa
Inclusion elastic modulus	$E_2 = E_1/r$ (r is the stiffness ratio)
Poisson's ratio	$\nu = 0.3$
Matrix and inclusion density	$\rho = 968.1$ kg/m^3
Inclusion loss factor	$\eta_c = 0.1, 0.6, 1.5$
Thickness	$h_v = 0.127$ mm
Whole beam dimensions	
Length	$L = 177.8$ mm
Thickness	$h = 3.175$ mm

Table 5
Material properties and dimensions of the beam with no damping.

Extreme layers	
Young's modulus	$E_0 = 69$ GPa
Poisson's ratio	$\nu = 0.3$
Density	$\rho_0 = 2766$ kg/m^3
Thickness	$h_0 = 1.524$ mm
Core layer	
Young's modulus	$E_c = 1794$ KPa
Poisson's ratio	$\nu = 0.3$
Density	$\rho_c = 968.1$ kg/m^3
Thickness	$h_c = 0.127$ mm
Whole beam dimensions	
Length	$L = 177.8$ mm
Thickness	$h = 3.175$ mm

assumption is no more valid. Nevertheless, this test shows the validity of this approach since the results of these two approaches are rather similar.

4.2. Sandwich beam

In this example, to demonstrate the efficiency of the multiscale approach to analyse the vibration of sandwich structures, we consider a three-layer cantilever sandwich beam (elastic/viscoelastic/elastic). The macrostructure has been discretized using a nine-node quadrangular element, while a three-node triangular element has been used to mesh the microstructures. The mesh of the macrostructure involves six elements (two elements per layer) through the thickness and 30 along the length (see Fig. 4). The material properties and dimensions of the beam are given in Table 4.

We study the influence of different parameters such as the stiffness ratio (r), the volume fraction ($v = V_2/V$; V_2 and V are the inclusion and the RVE volumes, respectively) and the inclusion morphology on the modal frequencies and modal damping. In the first two cases, the computed results have been compared with the obtained results from the study of a sandwich elastic beam with no inclusions; i.e. a beam with no damping (see Table 5). It allows understanding well the influence of various parameters on the damping and also, showing the capability of this method to design damping materials. The characteristics of the beam with no damping and different comparison results are displayed in Appendix A.

Moreover, in all examples, the variation of the loss factors and the frequencies of the first vibration mode according to the different studied parameters are only shown since different vibration modes have qualitatively the same variation.

4.2.1. Influence of the stiffness ratio

A biphasic RVE with circular inclusion (inclusion volume fraction of 20 percent) is considered. Fig. 5 shows the loss factors and the frequencies of the first vibration mode in function of the stiffness ratio for three values of the core loss factor: 0.1, 0.6 and 1.5. In both cases, the modal damping and the natural frequencies vary significantly when the stiffness ratio is between 0.1 and 10. When the core loss factor increases, the natural frequency increases and the modal damping of the structure decreases. The computed modal frequencies have been compared to the modal frequencies of a sandwich

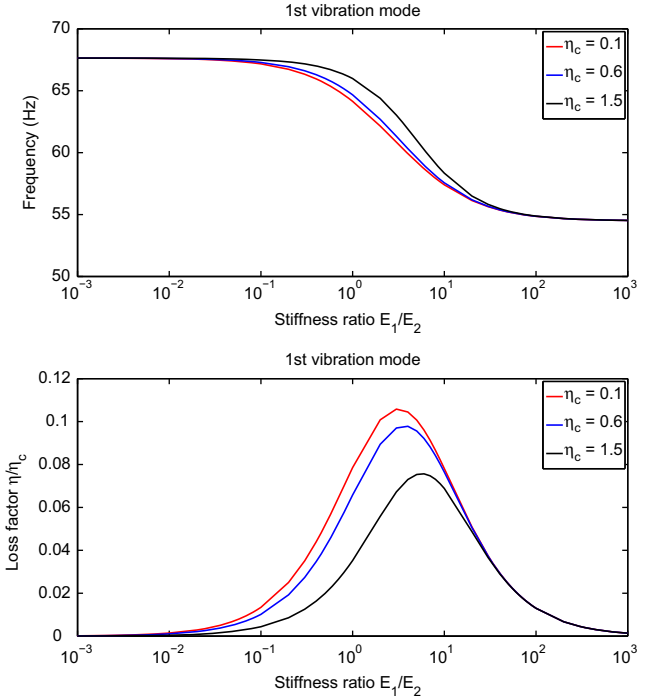

Fig. 5. Variation of modal damping and natural frequencies of the first vibration mode with respect to the stiffness ratio. Volume fraction $v=20\%$.

Table 6
Comparison of natural frequencies and modal damping: influence of stiffness ratio.

η_c	Beam with inclusions						Sandwich elastic beam with no damping
	$r=0.1$		$r=1$		$r=10$		
	f (Hz)	η/η_c	f (Hz)	η/η_c	f (Hz)	η/η_c	f (Hz)
0.1	66.3	0.010	64.1	0.056	59.4	0.053	64.1
	306.1	0.010	296.9	0.048	280.5	0.033	296.8
	760.4	0.007	745.3	0.030	721.0	0.018	745.2
	1414.6	0.004	1397.9	0.018	1372.4	0.009	1397.8
	2287.3	0.003	2269.9	0.011	2243.6	0.006	2269.8
0.6	66.4	0.007	64.5	0.047	59.5	0.052	64.1
	306.4	0.007	298.3	0.041	280.8	0.033	296.8
	761.1	0.005	747.5	0.027	721.3	0.017	745.2
	1415.2	0.003	1400.3	0.015	1372.7	0.009	1397.8
	2288.0	0.002	2272.3	0.010	2243.9	0.006	2269.8
1.5	66.5	0.003	65.5	0.025	60.0	0.047	64.1
	307.1	0.003	302.1	0.024	282.1	0.031	296.8
	762.2	0.002	753.7	0.016	723.0	0.017	745.2
	1416.5	0.001	1407.0	0.009	1374.4	0.009	1397.8
	2289.4	0.001	2279.4	0.006	2245.6	0.006	2269.8

elastic beam with no damping. A comparison between the obtained results for three values of the stiffness ratio (0.1, 1 and 10), is also shown in Table 6 in Appendix A.

4.2.2. Influence of the volume fraction

Like the previous example, we consider a biphasic RVE with circular inclusion, but, with different inclusion volume fractions: 20%, 40% and 60%. Fig. 6 displays the curves of variation of the modal damping and the natural frequencies of the first vibration mode according to the stiffness ratio for three considered volume fractions. The inclusion loss factor is equal to 0.6 for three volume fractions. The modal damping increases with the volume fraction, whatever the stiffness ratio value is. When the inclusion is more rigid than the matrix, increasing the volume fraction increases the natural frequency;

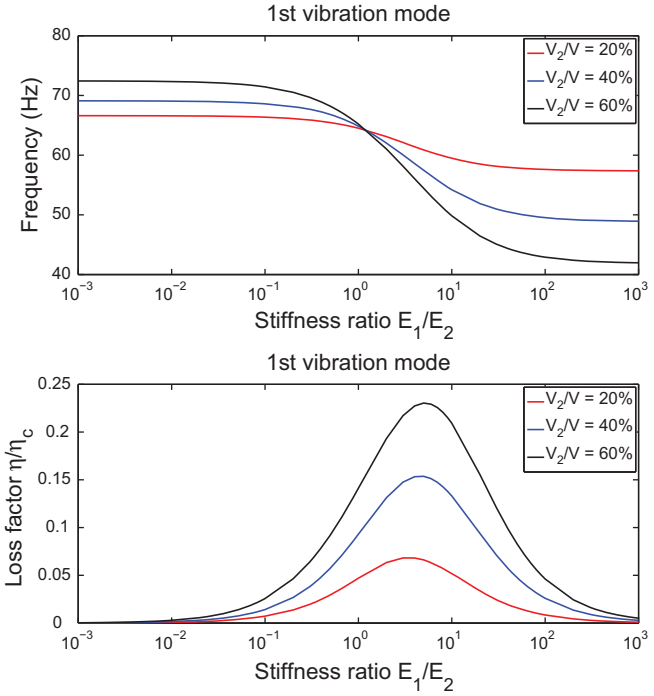

Fig. 6. Variation of modal damping and natural frequencies of the first vibration mode with loss factor $\eta_c = 0.6$. Three values of volume fraction are considered: 20%, 40% and 60%.

Table 7
Comparison of natural frequencies and modal damping: influence of the volume fraction—I.

η_c	Beam with inclusions: $r=0.1$						Sandwich elastic beam with no damping
	$v=20\%$		$v=40\%$		$v=60\%$		
	f (Hz)	η/η_c	f (Hz)	η/η_c	f (Hz)	η/η_c	f (Hz)
0.1	66.3	0.010	68.4	0.019	71.1	0.033	64.1
	306.1	0.010	316.9	0.022	333.5	0.049	296.8
	760.4	0.007	779.5	0.019	811.5	0.041	745.2
	1414.6	0.004	1436.2	0.010	1474.5	0.028	1397.8
	2287.3	0.003	2310.4	0.007	2351.8	0.019	2269.8
0.6	66.4	0.007	68.6	0.014	71.4	0.026	64.1
	306.4	0.007	317.7	0.017	335.4	0.039	296.8
	761.1	0.005	781.1	0.013	815.3	0.032	745.2
	1415.2	0.003	1438.1	0.008	1479.1	0.022	1397.8
	2288.0	0.002	2312.3	0.005	2357.0	0.015	2269.8
1.5	66.5	0.003	68.9	0.006	72.0	0.011	64.1
	307.1	0.003	319.3	0.007	339.4	0.018	296.8
	762.2	0.002	784.0	0.006	823.4	0.016	745.2
	1416.5	0.001	1441.5	0.004	1489.2	0.011	1397.8
	2289.4	0.001	2316.0	0.002	2368.1	0.008	2269.8

however, when the inclusion is less rigid than the matrix, increasing the volume fraction decreases the natural frequency. More results are shown in Tables 7–9 in Appendix A which display a comparison of natural frequencies and modal damping between the studied beam and a sandwich elastic beam with no damping for different stiffness ratios and volume fractions.

4.2.3. Influence of the morphology

We have studied three types of inclusion morphology: circular and, vertical and horizontal elliptical inclusions (see Fig. 7). The volume fraction is $v = 20\%$ and the core loss factor is $\eta_c = 0.6$. The ratio of the minor radius to the major one is 0.4 for the elliptical inclusions. Fig. 8 shows the curves of variation of the modal damping and natural frequencies for three types of morphology. The results of the horizontal and vertical elliptical inclusions are similar and different to those from circular inclusions. Indeed, the damping of three-layered sandwich structures with viscoelastic middle layer is mainly due to the shear deformation in the viscoelastic core especially when the faces are stiff [7–11, 29]. Moreover, although the effective stiffness tensors for two elliptical inclusions are anisotropic, with two different values along the principal directions of the ellipsoids, the obtained shear effective moduli in two cases are identical. Hence, the shear energy

Table 8
Comparison of natural frequencies and modal damping: influence of the volume fraction—II.

η_c	Beam with inclusions: $r=1$						Sandwich elastic beam with no damping
	$v=20\%$		$v=40\%$		$v=60\%$		
	f (Hz)	η/η_c	f (Hz)	η/η_c	f (Hz)	η/η_c	f (Hz)
0.1	64.1	0.056	64.1	0.112	64.2	0.168	64.1
	296.9	0.048	296.9	0.096	296.9	0.145	296.8
	745.3	0.030	745.3	0.061	745.3	0.092	745.2
	1397.9	0.018	1398.0	0.035	1398.0	0.053	1397.8
	2269.9	0.011	2269.9	0.023	2270.0	0.034	2269.8
0.6	64.5	0.047	64.9	0.093	65.2	0.141	64.1
	289.3	0.041	299.5	0.084	300.2	0.130	296.8
	747.5	0.027	749.2	0.055	749.9	0.085	745.2
	1400.3	0.015	1402.1	0.032	1402.6	0.050	1397.8
	2272.3	0.010	2274.2	0.020	2274.7	0.032	2269.8
1.5	65.5	0.025	66.8	0.049	68.0	0.078	64.1
	302.1	0.024	307.2	0.051	311.0	0.088	296.8
	753.7	0.016	761.7	0.035	767.0	0.063	745.2
	1407.0	0.009	1415.6	0.021	1420.7	0.038	1397.8
	2279.4	0.006	2288.3	0.014	2293.4	0.025	2269.8

Table 9
Comparison of natural frequencies and modal damping: influence of the volume fraction—III.

η_c	Beam with inclusions: $r=10$						Sandwich elastic beam with no damping
	$v=20\%$		$v=40\%$		$v=60\%$		
	f (Hz)	η/η_c	f (Hz)	η/η_c	f (Hz)	η/η_c	f (Hz)
0.1	59.4	0.053	53.9	0.137	49.4	0.217	64.1
	280.5	0.033	266.5	0.062	257.6	0.075	296.8
	721.0	0.018	703.2	0.027	693.2	0.029	745.2
	1372.4	0.006	1354.5	0.014	1344.8	0.014	1397.8
	2243.6	0.006	2225.5	0.009	2215.9	0.009	2269.8
0.6	59.5	0.052	54.2	0.133	49.8	0.209	64.1
	280.8	0.033	267.0	0.061	258.0	0.074	296.8
	721.3	0.017	703.5	0.027	693.5	0.029	745.2
	1372.7	0.009	1354.9	0.014	1345.0	0.014	1397.8
	2243.9	0.006	2225.9	0.009	2216.1	0.009	2269.8
1.5	60.0	0.047	55.6	0.115	51.7	0.177	64.1
	282.1	0.031	269.2	0.057	260.3	0.069	296.8
	723.0	0.017	705.5	0.026	695.0	0.028	745.2
	1374.4	0.009	1356.7	0.014	1346.4	0.014	1397.8
	2245.6	0.006	2227.7	0.008	2214.4	0.009	2269.8

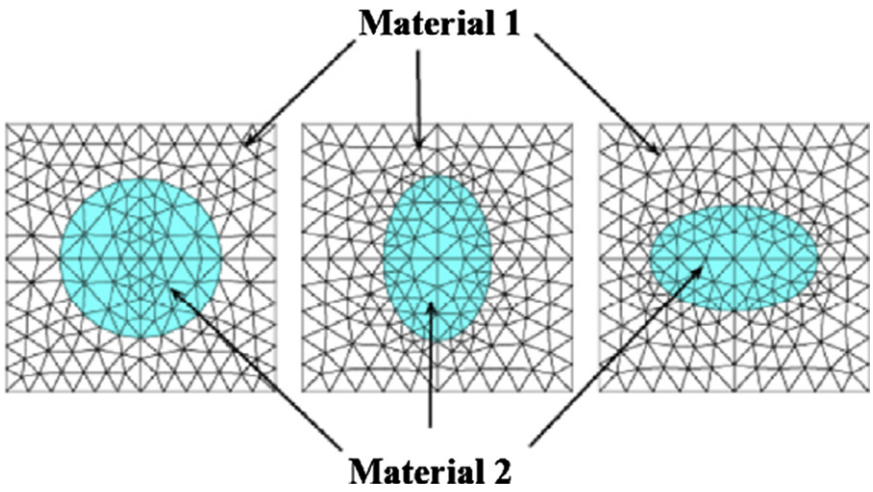

Fig. 7. Biphasic RVE with circular and, vertical and horizontal elliptical inclusions; volume fraction $v=20\%$.

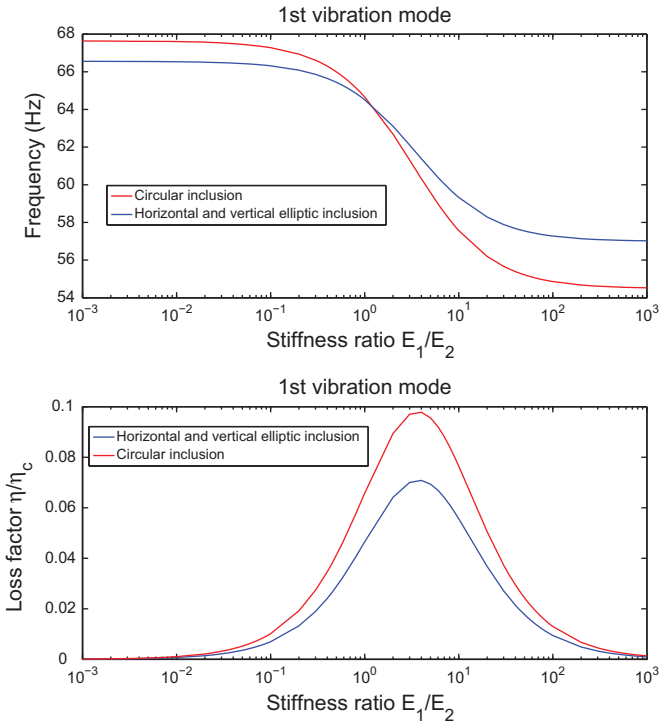

Fig. 8. Variation of modal damping and natural frequencies of the first vibration mode with loss factor $\eta_c = 0.6$ for three considered morphologies for the sandwich beam; volume fraction $v=20\%$.

developed by the biphasic RVEs with horizontal and vertical elliptical is the same and differs to that in the RVE with circular inclusions. Note that a higher modal damping properties can be obtained from sandwich beam with circular inclusions. The natural frequencies of circular inclusion are higher than those of elliptical inclusions when the inclusion is more rigid than the matrix; but, when the rigidity ratio is increased, the natural frequencies of circular inclusion are lower than those of elliptical inclusions.

To show well the influence of morphology, a heterogeneous beam like the first example is considered. The material properties are the same as the viscoelastic core layer in the sandwich structure. Moreover, in our study, the ratio between the minor and major radii of elliptical inclusion (b/a) (see Fig. 9) is taken into account by fixing the inclusion volume fraction of $v=20\%$. Fig. 10 shows the loss factors and the frequencies of the first vibration mode in function of the stiffness

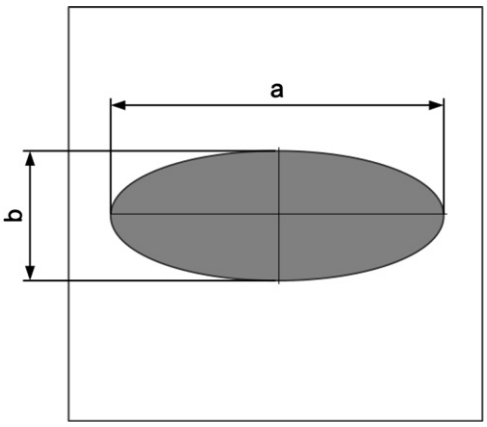

Fig. 9. Biphasic RVE with elliptical inclusion.

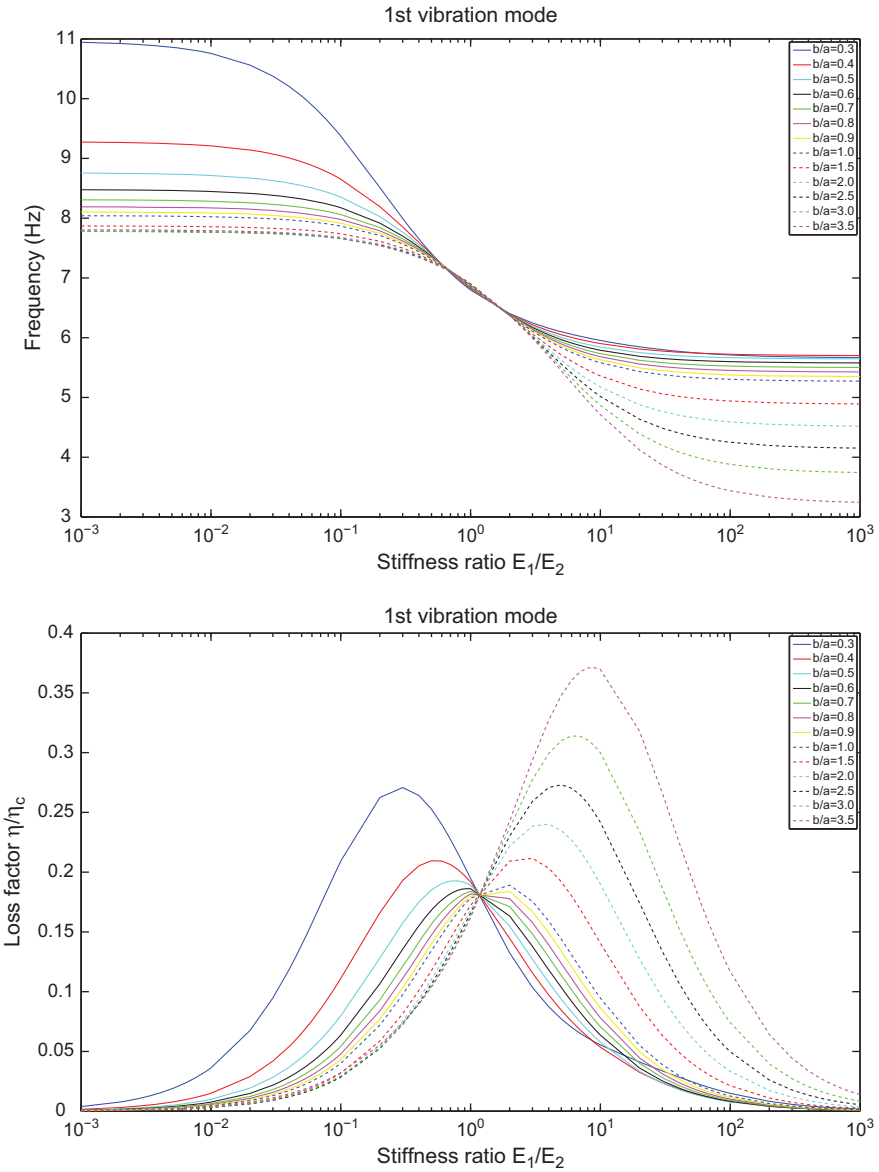

Fig. 10. Variation of modal damping and natural frequencies of the first vibration mode with loss factor $\eta_c = 0.6$ for different values of b/a for the heterogeneous beam; volume fraction $v = 20\%$.

ratio for different values of b/a. The beams with $b/a<1$ (horizontal elliptical inclusions) have always higher natural frequencies. The values of modal damping of the beams with $b/a>1$ (vertical elliptical inclusions) are higher when the inclusion is less rigid than the matrix; but, when the rigidity ratio is decreased, the beams with $b/a<1$ (horizontal elliptical inclusions) have higher values of modal damping. The results of the circular inclusion ($b/a=1$) are normally between ones of vertical and horizontal elliptical inclusions.

5. Conclusion

Based on the multiscale approach, a numerical method has been proposed for vibration analysis of sandwich structures with viscoelastic inclusions. It consists in computing numerically the effective properties by solving a finite element problem at the microscopic scale and the damping properties (loss factor and frequency) by solving a complex eigenvalue problem at the macroscopic scale. In this way, we can study the influence of different parameters on the passive damping of the structure such as the morphology, the stiffness ratio and volume fraction of the viscoelastic inclusion. However, this approach is limited to the low or medium frequency range because of neglecting inertia effects at the microscopic scale. Numerical examples have been presented to validate the approach and to estimate the loss factor in the case of sandwich structure with constant complex modulus for instance. This method can be very useful in the design of sandwich structures with optimized damping properties. Ongoing work concerns the development of a procedure in which the microscopic inertia effects and the more general viscoelastic models are taken into account.

References

[1] M. Trindade, A. Benjeddou, Hybrid active–passive damping treatments using viscoelastic and piezoelectric materials: *review and assessment*, *Journal of Vibration and Control* 8 (2002) 699–745.
[2] E.M. Kerwin, Damping flexural waves by constrained viscoelastic layer, *Journal of the Acoustical Society of America* 31 (1959) 952–962.
[3] M. Soni, Finite element analysis of viscoelastically damped sandwich structures, *Shock and Vibration Bulletin* 55 (1981) 97–109.
[4] K.J. Bathe, *Finite Element Procedures in Engineering Analysis*, Prentice Hall, 1982.
[5] J.-H. Wilkinson, *The Algebraic Eigenvalue Problem*, Oxford University Press, 1965.
[6] R. Rikards, A. Chate, E. Barkanov, Finite element analysis of damping the vibrations of laminated composites, *Computers and Structures* 47 (1993) 1005–1015.
[7] B.A. Ma, J.F. He, Finite element analysis of viscoelastically damped sandwich plates, *Journal of Sound and Vibration* 52 (1992) 107–123.
[8] X. Chen, H.L. Chen, L.E. Hu, Damping prediction of sandwich structures by order-reduction-iteration approach, *Journal of Sound and Vibration* 222 (1999) 803–812.
[9] E.M. Daya, M. Potier-Ferry, A numerical method for nonlinear eigenvalue problems: *application to vibrations of viscoelastic structures*, *Computers and Structures* 79 (2001) 533–541.
[10] L. Duigou, E.M. Daya, M. Potier-Ferry, Iterative algorithms for nonlinear eigenvalue problems: *application to vibrations of viscoelastic shells*, *Computer Methods in Applied Mechanics and Engineering* 192 (2003) 1323–1335.
[11] H. Boudaoud, S. Belouettar, E.M. Daya, M. Potier-Ferry, A numerical method for nonlinear complex modes with applications to active–passive damped sandwich structures, *Engineering Structures* 31 (2009) 284–291.
[12] R.K. Patel, B. Bhattacharya, S. Basu, A finite element based investigation on obtaining high material damping over a large frequency range in viscoelastic composites, *Journal of Sound and Vibration* 303 (2007) 753–766.
[13] Y. Koutsawa, M. Cherkaoui, E.M. Daya, Multicoating inhomogeneities problem for effective viscoelastic properties of particulate composite materials, *Journal of Engineering Materials and Technology* 131 (2009) 2–11.
[14] P. Suquet, *Homogenization Techniques for Composites Materials, Lecture Notes in Physics*, vol. 272, Springer, Berlin, 1987 (pp. 193–278).
[15] S. Nemat-Nasser, M. Hori, Micromechanics: overall properties of heterogeneous materials, North-Holland Series, Applied Mathematics and Mechanics, vol. 37, North-Holland, Amsterdam, 1993.
[16] F. Feyel, J. Chaboche, FE^2 multiscale approach for modeling the elastoviscoplastic behavior of long fiber SiC/Ti composite materials, *Computer Methods in Applied Mechanics and Engineering* 183 (2000) 309–330.
[17] V. Kousnetzova, M. Geers, W. Brekelmans, Multi-scale second order computational homogenization of multi-phase materials: *a nested finite element solution strategy*, *Computer Methods in Applied Mechanics and Engineering* 193 (2004) 5525–5550.
[18] S. Nezamabadi, J. Yvonnet, H. Zahrouni, M. Potier-Ferry, A multilevel computational strategy for microscopic and macroscopic instabilities, *Computer Methods in Applied Mechanics and Engineering* 198 (2009) 2099–2110.
[19] P. Kanouté, D.P. Boso, J.L. Chaboche, B.A. Schrefler, Multiscale methods for composites: *a review*, *Archives of Computational Methods in Engineering* 16 (2009) 31–75.
[20] S. Nezamabadi, H. Zahrouni, J. Yvonnet, M. Potier-Ferry, A multiscale finite element approach for buckling analysis of elastoplastic long fiber composites, *International Journal for Multiscale Computational Engineering* 8 (2010) 287–301.
[21] R.M. Christensen, Viscoelasticproperties of heterogeneous media, *Journal of the Mechanics and Physics of Solids* 17 (1969) 23–41.
[22] M. Koishi, M. Shiratori, T. Miyoshi, K. Kabe, Homogenization method for dynamic viscoelastic analysis of composite materials, *JSME International Journal Series A* 40 (1997) 306–312.
[23] Y.M. Yi, S.H. Park, S.K. Youn, Asymptotic homogenization of viscoelastic composites with periodic microstructures, *International Journal of Solids and Structures* 17 (1998) 2039–2055.
[24] Y.M. Yi, S.H. Park, S.K. Youn, Design of microstructures of viscoelastic composites for optimal damping characteristics, *International Journal of Solids and Structures* 37 (2000) 4791–4810.
[25] P.W. Chung, K.K. Tamma, R.R. Namburu, A micro/macro homogenization for viscoelastic creep analysis with dissipative correctors for heterogeneous woven-fabric layered media, *Composite Science and Technology* 60 (2000) 2233–2253.
[26] G. Dai, W. Zhang, Cell size effects for vibration analysis and design of sandwich beams, *Acta Mechanica Sinica* 25 (2009) 353–365.
[27] H.H. Zhang, L.X. Li, Modeling inclusion problems in viscoelastic materials with the extended finite element method, *Finite Elements in Analysis and Design* 45 (2009) 721–729.
[28] A. Arau´ jo, C.M. Soares, J. Herskovits, P. Pedersen, Estimation of piezoelastic and viscoelastic properties in laminated structures, Composite Structures 87 (2009) 168–174.
[29] C. Johnson, D. Kienholz, L. Rogers, Finite element prediction of damping in beams with constrained viscoelastic layers, Shock and Vibration Bulletin 51 (1981) 71–81.
[30] C. Miehe, Computational micro-to-macro transitions for discretized micro-structures of heterogeneous materials at finite strains based on the minimization of averaged incremental energy, Computer Methods in Applied Mechanics and Engineering 192 (2003) 559–591.